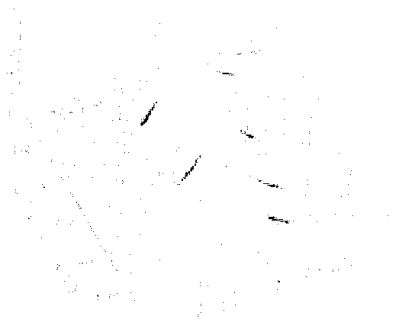

QFA5 Fig. 1. Space-time evolution of a slow Raman gap soliton.

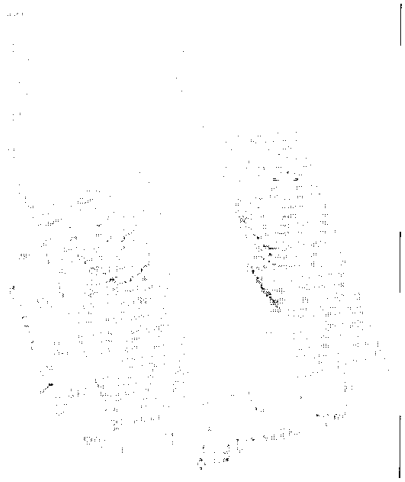

QFA5 Fig. 2. Stationary Raman gap soliton.

We take into account self- and cross-phase modulation, Raman gain, and pump depletion. The equations are:

$$\frac{\delta A_p}{\delta z} + \frac{1}{v_p}\frac{\delta A_p}{\delta t} = -\frac{g_p}{2}(|A_{s+}|^2 + |A_{s-}|^2)A_p + i\gamma_p(|A_p|^2 + 2|A_{s+}|^2 + 2|A_{s-}|^2)A_p, \quad (1)$$

$$\frac{\delta A_{s+}}{\delta z} + \frac{1}{v_s}\frac{\delta A_{s+}}{\delta t} = -\frac{g_s}{2}|A_p|^2 A_{s+} + i\gamma_s(|A_{s+}|^2 + 2|A_p|^2 + 2|A_{s-}|^2)A_{s+} + i\kappa A_{s-} + i\Delta\beta A_{s+}, \quad (2)$$

$$\frac{\delta A_{s-}}{\delta z} - \frac{1}{v_s}\frac{\delta A_{s-}}{\delta t} = -\frac{g_s}{2}|A_p|^2 A A_{s-} - i\gamma_s(|A_{s-}|^2 + 2|A_p|^2 + 2|A_{s+}|^2)A_{s-} - i\kappa A_{s+} - i\Delta\beta A_{s-}. \quad (3)$$

Here κ is the grating coupling constant, $\Delta\beta$ is the detuning from the Bragg resonance, the γ's are nonlinear index coefficients, and the g's are Raman gain coefficients.

Figure 1 shows the evolution of a slow Raman gap soliton with a velocity only 1% the speed of light in the unperturbed medium.

Stable, immobile Raman gap solitons have also been found for certain parameter values. Fig. 2 shows such a stable, stationary gap soliton. For this soliton the amplitudes of the forward and backward components are equal. The lifetime of this soliton is at least 20 nanoseconds, which is forty times the duration of the pump pulse. The steady state Raman gap soliton is accurately described by a sech^2 profile.

1. H.G. Winful, J.H. Marburger, and E. Garmire, "Theory of bistability in nonlinear distributed feedback structures," Appl. Phys. Lett. **35,** 376–378 (1979).
2. H.G. Winful and G.D. Cooperman, "Self-pulsing and chaos in distributed feedback bistable optical devices," Appl. Phys. Lett. **40,** 298–300 (1982).
3. H.G. Winful, "Pulse compression in optical fiber filters," Appl. Phys. Lett. **46,** 527–529 (1985).
4. D.N. Christodoulides and R.I. Joseph, "Slow Bragg solitons in nonlinear periodic structures," Phys. Rev. Lett. **62,** 1746–1749 (1989).
5. W. Chen and D.L. Mills, "Gap solitons and nonlinear optical response of superlattices," Phys. Rev. Lett. **58,** 160–163 (1987).
6. B.J. Eggleton, C.M. de Sterke, and R.E. Slusher, "Nonlinear pulse propagation in Bragg gratings," J. Opt. Soc. Am. B **14,** 2980–2993 (1997).

QFA6 9:30 am

Co-linear anti-Stokes generation from a cw Raman laser

J.K. Brasseur, P.A. Roos,* L.S. Meng,* J.L. Carlsten,* *US Air Force Academy; E-mail: Jay.Brasseur@usafa.af.mil*

Using the high optical power build-up within a high finesse cavity (HFC), two-photon nonlinear processes have recently been studied with low power cw lasers. In particular, stimulated Raman scattering has been used to construct non-resonant cw Raman lasers with high efficiencies and pump thresholds on the order of $1\mathrm{mW}^{-1}$. Although this study was limited to Stokes emission, parametric processes such as coherent anti-Stokes scattering are also possible. In the pulsed laser regime, anti-Stokes commonly emits in ring patterns due to phase matching requirements. More recently, however, co-linear emission of pulsed anti-Stokes was observed in solid H_2 through self-induced phase matching[2]. We report the observation of co-linear cw anti-Stokes emission from a cw Nd:YAG-pumped Raman laser in H_2 gas.

Anti-Stokes emission is a result of a parametric four-wave mixing process. The growth of the resulting anti-Stokes field can be shown to depend on the pump and Stokes fields present inside the HFC in the following manner[3]

$$E_{as} = -\frac{1}{2}\sqrt{T_{as}}\,\frac{C_{as}^{4W}E_p E_p E_s^*}{L_{as}}, \quad (1)$$

where E_{as} is the anti-Stokes field exiting the HFC and E_p, and E_s are the field amplitudes for the pump, and Stokes beams inside the HFC respectively. The coupling of the pump and

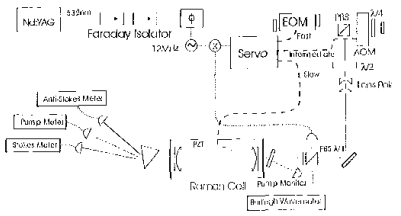

QFA6 Fig. 1. Experimental apparatus used to measure the anti-Stokes emission. The Nd:YAG laser frequency is controlled via an acousto-optic modulator (AOM) and an electro-optic modulator (EOM). HFC drifts are corrected using a piezo electric transducer separating the cavity mirrors.

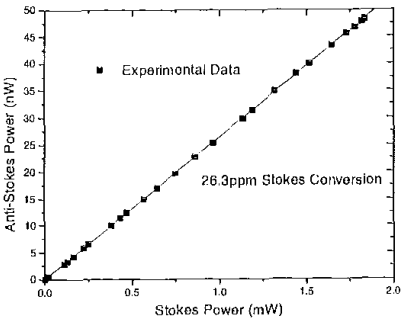

QFA6 Fig. 2. Anti-Stokes output power as a function of Stokes output power on the Raman line-center.

Stokes fields including phase-matching is represented by C_{AS}^{4W}. Interferometric effects of the cavity at the anti-Stokes frequency can be accounted for by including the following cavity factor:

$$C(F,\delta) = \frac{1}{1 + F\cdot\sin^2\frac{\delta}{2}} \quad (2)$$

where $F = 4R_{as}/(1 - R_{as})^2$, *and* $\delta = \pi c/l(\Delta + \phi)$. ϕ corresponds to the relative frequency difference between the Raman line-center and the anti-Stokes cavity resonance and Δ is the tuning of the pump frequency from the Raman line-center.

Figure 1 shows the experimental apparatus. The cw Raman laser is optically pumped by a frequency-doubled Nd:YAG laser with single mode operation at 532nm and up to 200 mW of optical power. The beam is sent through a resonant phase modulator to place sidebands on the carrier frequency, which are used for phase/frequency locking of the HFC and the pump laser. A prism spatially separates the pump (532 nm), Stokes (683 nm) and anti-Stokes (436 nm) beams at the exit of the cavity for detection purposes.

Figure 2 shows the output power of the anti-Stokes emission as a function output Stokes power on the Raman line-center. Growth of the anti-Stokes power is linear with respect to that of the Stokes, as predicted by Eqn. 1. The measured ratio of the Stokes to anti-Stokes optical power is 26.3 ppm. The anti-Stokes emission is observed to be collinear to the pump and Stokes beams with a Gaussian spatial profile.

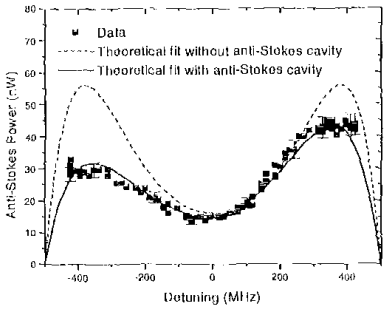

QFAG Fig. 3. Anti-Stokes emission as a function of detuning from the Raman line-center. The solid (dashed) line shows the predictions with (without) Eqn. 2 included.

Figure 3 shows the anti-Stokes emission as a function of detuning from the Raman resonance line-center for a constant pump power of 3.2 mW (4 × threshold for detuning = 0). The data is in good agreement with the theoretical predictions of Eqn. 1 when the interferometric effects of Eqn. 2 are included (solid line). Note that the anti-Stokes emission can actually increase with detuning from the Raman resonance since this also raises the laser threshold, thereby allowing more pump to contribute to the four-wave process. We have therefore introduced a theory that accurately describes the behavior of coherent anti-Stokes emission from a cw Raman laser.

This work is supported by NSF under grant #9731602.

*Montana State Univ., U.S.A.

1. J.K. Brasseur, K.S. Repasky, and J.L. Carlsten, "Continuous-wave Raman laser in H_2" Opt. Lett. **23,** 367 (1998).
2. K. Hakuta, M. Suzuki, M. Katsuragawa, and J.Z. Li, Phys. Rev. Lett. **79,** 209 (1997).
3. J.K. Brasseur, P.A. Roos, K.S. Repasky and J.L. Carlsten, "Coherent Anti-Stokes Emission in a Continuous Wave Raman Laser in H_2" Submitted to J. Opt. Am. B (1999).

QFB

8:00 am–9:45 am
Room 270–276

Ultrafast Electronic Dynamics of Molecules

Shaul Mukamel, *Univ. of Rochester, USA, Presider*

QFB1 **8:00 am**

Direct observation of the ultrafast electron transfer process in a polymer/fullerene blend

G. Cerullo, G. Lanzani, S. De Silvestri, Ch.J. Brabec,* G. Zerza,* N.S. Sariciftci,* J.C. Hummelen,** *Istituto Nazionale per la Fisica della Materia, Milan, Italy; E-mail: giulio.cerullo@polimi.it*

Photoinduced electron transfer in organic molecules is an extensively investigated topic both because of fundamental interest in the photophysics and for applications to artificial photosynthesis. Highly efficient ultrafast electron transfer from photoexcited conjugated polymers to C_{60} has been reported,[1] the back transfer is heavily hindered, thus providing an intrinsic stabilization mechanism of the photogenerated charges. Although an upper limit for the forward electron transfer time of 1 ps has been reported,[2] its detailed time resolution is still missing and is highly needed to shed light on the photophysics of the charge transfer mechanism.

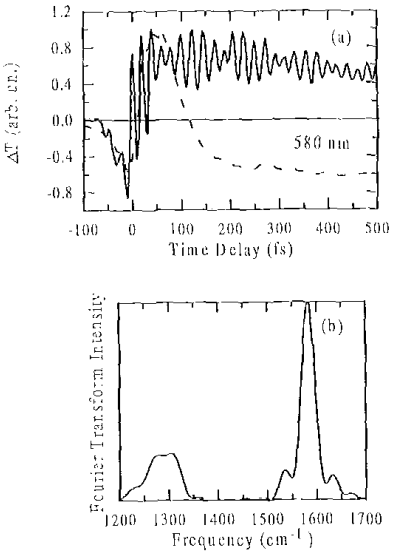

QFB1 Fig. 1. (a) Differential transmission dynamics for pure MDMO-PPV (solid line) and PPV/C_{60} (dashed line) at the probe wavelength of 580 nm; (b) Fourier transform of oscillatory component of the MDMO-PPV signal.

In this work we perform ultrafast experiments on conjugated polymer/C_{60} blends with sub-10-fs time resolution. We are able to time resolve for the first time the charge transfer process, obtaining a forward electron transfer time constant $\tau_{et} \approx 45$ fs.

The excitation source is a visible optical parametric amplifier[3,4] providing ultrabroadband pulses with sub-10-fs duration and spectrum extending from 520 to 720 nm. Pump-probe measurements are performed in a noncollinear configuration and single probe wavelengths are selected using interference filters after the sample. We excite thin films of poly [2-methoxy, 5-(3′,7′-dimethyl-octyloxy)]-p-phenylene vinylene (MDMO-PPV) blended with C_{60}, with a 1:1 ratio in molecular concentration; at these high C_{60} concentrations diffusion doesn't influence the dynamics and we measure the intrinsic charge transfer process. We also study, for comparison, pure films of MDMO-PPV.

Fig. 1(a) shows as solid line the differential transmission (ΔT) signal for pure MDMO-PPV at the probe wavelength of 580 nm. The features at negative and near-zero delays at this and other wavelengths are due to coherent artifacts. The ΔT signal has positive sign and, because of negligible ground state absorption at this wavelength, is assigned to stimulated emission from the excited state. The strong oscillations superimposed on the signal are due to the motion of the vibrational wavepacket launched by the pump pulse on the excited state potential energy surface and thus probe the vibrational modes coupled to the excited state. A Fourier transform of the oscillatory component of the signal is shown in Fig. 1(b). By adding C_{60} to the polymer matrix, the signal changes dramatically (dashed line in Fig. 1(a)). The initially positive ΔT changes rapidly sign, indicating the quick formation of a new photoinduced absorption (PA), which remains then stationary on the timescale of the experiment. Based on cw PA measurements, this new absorption is assigned to the MDMO-PPV charged state (polaron) and thus provides a direct signature for the charge transfer process. By an exponential fitting of the PA rise-time, a time constant for the electron transfer process of ≈45 fs is calculated. Similar results are obtained at other probe wavelengths, as shown in Fig. 2.

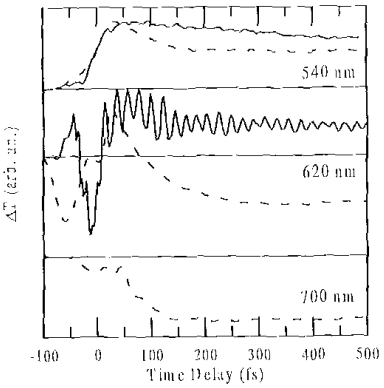

QFB1 Fig. 2. Differential transmission dynamics for pure MDMO-PPV (solid line) and PPV-C_{60} (dashed line) at different probe wavelengths.

Excited state vibrational coherence is not maintained in the charge transfer process, thus indicating evolution of the system on an anharmonic charge transfer potential energy surface, formed immediately after photoexcitation.[5] Such a fast charge transfer can only be explained by a strong ($\Delta E \approx \hbar/\tau \approx 90$ meV) exchange integral of the excited state orbitals of donor and acceptor molecules and requires detailed theoretical analysis to clarify its physical mechanism.

*University of Linz, Austria
**University of Groningen, The Netherlands

1. N.S. Sariciftci, L. Smilowitz, A.J. Heeger, and F. Wudl, "Photoinduced electron transfer from a conducting polymer to buckminsterfullerene", Science **258,** 1474–1477 (1992).
2. B. Kraabel, D. McBranch, N.S. Sariciftci, D. Moses, A.J. Heeger, "Ultrafast spectroscopic studies of photoinduced electron transfer from semiconducting polymers to C_{60}", Phys. Rev. B **50,** 18543–18552 (1994).
3. G. Cerullo, M. Nisoli, S. Stagira, S. De Silvestri, "Sub-8-fs pulses from an ultrabroadband optical parametric amplifier in the visible", Opt. Lett. **23,** 1283–1285 (1998).